

Article

Improved Hydrogenation Kinetics of TiMn_{1.52} Alloy Coated with Palladium through Electroless Deposition

Thabang R. Somo¹, Moegamat W. Davids², Mykhaylo V. Lototsky^{2,*} , Mpitloane J. Hato¹ 
and Kwena D. Modibane^{1,*} 

¹ Department of Chemistry, School of Physical and Mineral Sciences, University of Limpopo (Turfloop), Polokwane, Sovenga 0727, South Africa; somoronny@gmail.com (T.R.S.); mpitloane.hato@ul.ac.za (M.J.H.)

² HySA System, South African Institute for Advanced Material Chemistry, University of the Western Cape, Bellville, Cape Town 7535, South Africa; mwdavids@uwc.ac.za

* Correspondence: mlototsky@uwc.ac.za (M.V.L.); kwena.modibane@ul.ac.za (K.D.M.)

Abstract: The deterioration of hydrogen charging performances resulting from the surface chemical action of electrophilic gases such as CO₂ is one of the prevailing drawbacks of TiMn_{1.52} materials. In this study, we report the effect of autocatalytic Pd deposition on the morphology, structure, and hydrogenation kinetics of TiMn_{1.52} alloy. Both the uncoated and Pd-coated materials were characterized using scanning electron microscopy/energy dispersive spectroscopy (SEM/EDS) and X-ray diffraction (XRD). XRD analyses indicated that TiMn_{1.52} alloy contains C14-type Laves phase without any second phase, while the SEM images, together with a particle size distribution histogram, showed a smooth non-porous surface with irregular-shaped particles ranging in size from 1 to 8 μm. The XRD pattern of Pd-coated alloy revealed that C14-type Laves phase was still maintained upon Pd deposition. This was further supported by calculated crystallite size of 29 nm for both materials. Furthermore, a Sieverts-type apparatus was used to study the kinetics of the alloys after pre-exposure to air and upon vacuum heating at 300 °C. The Pd-coated AB₂ alloy exhibited good coating quality as confirmed by EDS with enhanced hydrogen absorption kinetics, even without activation. This is attributed to improved surface tolerance and a hydrogen spillover mechanism, facilitated by Pd nanoparticles. Vacuum heating at 300 °C resulted in removal of surface barriers and showed improved hydrogen absorption performances for both coated and uncoated alloys.

Keywords: hydrogen storage materials; AB₂ alloys; TiMn_{1.52} alloy; palladium deposition



Citation: Somo, T.R.; Davids, M.W.; Lototsky, M.V.; Hato, M.J.; Modibane, K.D. Improved Hydrogenation Kinetics of TiMn_{1.52} Alloy Coated with Palladium through Electroless Deposition. *Materials* **2021**, *14*, 1833. <https://doi.org/10.3390/ma14081833>

Academic Editor: Eli Grigorova

Received: 5 March 2021

Accepted: 22 March 2021

Published: 7 April 2021

Publisher's Note: MDPI stays neutral with regard to jurisdictional claims in published maps and institutional affiliations.



Copyright: © 2021 by the authors. Licensee MDPI, Basel, Switzerland. This article is an open access article distributed under the terms and conditions of the Creative Commons Attribution (CC BY) license (<https://creativecommons.org/licenses/by/4.0/>).

1. Introduction

AB₂-type Laves phase alloys are an attractive class of metal hydrides due to their better reversible absorption and desorption of hydrogen, good activation property, and low cost [1,2]. The most studied and promising AB₂-type alloy materials are the Ti–Mn binary alloys [3–5]. Because of their light weight, Ti–Mn binary alloys possess a large hydrogen absorption capacity of more than 1.0 hydrogen to metal ratio (H/M) and moderate equilibrium plateau pressure (reported to be 0.7 MPa) under near ambient temperatures as compared to other AB₂ alloys [6]. Regardless of these superior properties, deterioration of hydrogen charging performances resulting from the surface chemical action of poisonous electrophilic gases is still a concern and therefore activation prior to hydrogen absorption is required [1,7]. Some well-known attempts to improve hydrogenation behaviour of these binary alloys include element substitution, structural change, and multicomponent strategies [6,8]. An example of element substitution includes a study by Liu et al. [1], where Ti and Zr comprised the A site, while Mn, Cr, V, Ni, Fe, and Cu metals occupied the B site to produce a (Ti_{0.85}Zr_{0.15})_{1.05}Mn_{1.2}Cr_{0.6}V_{0.1}M_{0.1} alloy (where M=Ni, Fe, Cu). This material showed a great improvement in cyclability but poor hydrogenation kinetics due to its poor poisoning-resistance. Other improvements of the hydrogenation behaviour

have been previously reported through surface protecting techniques such as microencapsulation [9,10], coating with metal oxides [11], and fluorination treatment [12]. All these techniques have high and low affinity for hydrogen and poisonous gases, respectively, but their limitations are not avoidable. For instance, the microencapsulation technique, which involves coating of the bulk alloy with 10 wt.% of Ni or Cu, utilises large amounts of the coating metal that is not responsible for hydrogen storage. It is also not economically favoured and produces heavy metal alloys [10]. On the other hand, surface modification through deposition of platinum group metals (PGMs), particularly palladium (Pd) which has a strong affinity for hydrogen, has been reported to possess relatively favourable and efficient improvement towards hydrogenation properties of alloy materials [13,14]. The effect of Pd on hydrogenation properties of alloy materials has been studied intensively over the years. For example, a study by Zaluska et al. [15] showed that, to some extent, Pd coating on AB, A₂B, and AB₅ alloy materials promoted fast hydrogen absorption, with a small or no incubation period. Similar observations were shared by Uchida et al. [16] when Pd nanoparticles were deposited on the surface of titanium films. In this investigation, autocatalytic palladium deposition was identified for surface modification of TiMn_{1.52} alloy; its effect on hydrogen sorption kinetics after exposure to air was then studied using a Sieverts-type apparatus. To the best of our knowledge, such studies on hydrogenation kinetics of Pd-coated TiMn_{1.52} alloy do not appear to have been reported yet.

2. Experimental Methods

2.1. Materials

The AB₂-type (TiMn_{1.52}) hydride-forming alloy was prepared from Ti (99.9%) and Mn (99.9%) purchased from Sigma Aldrich (St. Louis, MO, USA). The AB₂ hydride forming alloy was prepared by arc-melting on a water-cooled copper crucible in a protective argon atmosphere. All prepared ingots were melted three times to provide homogeneity. Subsequently, the prepared metal ingots were pulverised by ball-milling in argon for 10 min. The material was allowed constant exposure to air throughout the experimental studies.

2.2. Surface Modification of Alloy

Surface modification of the TiMn_{1.52} alloy was conducted through autocatalytic deposition of Pd in a hypophosphite-based autocatalytic plating bath following the procedure described here [17]. Prior to palladium deposition, the materials were first sensitized and activated in a palladium–tin (Pd–Sn) colloidal solution [17] resulting in increased densities of Pd deposition and surface Pd loading on the intermetallide. The activated intermetallide was subsequently suspended in the palladium plating bath. An equivalent volume of NaH₂PO₂ solution (10 g/L) was added separately. The plating time and stirring rate were fixed at 30 min and 300 rpm, respectively. The main purpose of surface coating with Pd was to improve the poisoning-tolerance of the material as well as to form a material with excellent hydrogen sorption properties. The autocatalytic deposition of Pd was applied to a ~5 g batch of TiMn_{1.52} alloy.

2.3. Characterisation Techniques

X-ray diffraction (XRD) studies of the alloys were performed using a Bruker Advance powder diffractometer (Madison, WI, USA; 40 mA, 40 keV) at the Materials Research Group, iThemba Labs, in Cape Town, South Africa for phase identification. The XRD analysis was done with an X-ray source of Cu K α radiation ($\lambda = 1.5406 \text{ \AA}$).

Scanning electron microscopes/energy-dispersive spectroscopy (SEM/EDS, Edax Genesis, Tilburg, The Netherlands, 100 live seconds) studies were carried out using a Leo 1450 microscope (Carl Zeiss, Jena, Germany) (20 kV, secondary electrons) at the Physics department, University of the Western Cape (UWC) to evaluate the morphology of AB₂-type alloy particle size/shape, Pd particle dispersion on the surface of the AB₂-type alloy particles, and Pd particle size/shape.

The effect of autocatalytic palladium deposition on hydrogenation kinetics of $\text{TiMn}_{1.52}$ alloy was evaluated by a comparison of hydrogen absorption after pre-exposure to air and hydrogen absorption after vacuum heating at 300 °C. Vacuum heating facilitates the removal of any existing oxide layers on the surface of the alloy. Hydrogen absorption was conducted using a commercial Sieverts-type volumetric installation (PCTPro-2000, Hy-Energy LLC, California, CA, US) at the South African Institute for Advanced Material Chemistry (SAIAMC), UWC. The measurements were carried out at $T = 20$ °C, $P_0 \sim 30$ bar H_2 , for 2 h. The experimental results were processed by application of formal kinetic analysis, using the Avrami–Erofeev Equation (1) [18]

$$\left(\frac{H}{AB_2}\right) = \left(\frac{H}{AB_2}\right)_{\max} \times \{1 - \exp(-kt^n)\} \quad (1)$$

where (H/AB_2) is the actual hydrogen concentration in the alloy, $(H/AB_2)_{\max}$ is the maximum hydrogen concentration in the alloy, t is time, k represents rate constant, and the index of power, n , is interpreted as a value indirectly connected to the reaction mechanism.

3. Results and Discussion

3.1. Structural Characterisation

Figure 1 shows the XRD patterns of Pd-coated and uncoated $\text{TiMn}_{1.52}$ alloys. The XRD analyses indicate that $\text{TiMn}_{1.52}$ alloy exhibits a disordered structure and C14-type Laves phase without any second phase. C14-type Laves phase of the same alloy was previously reported by Dekhtyarenko et al. [19] and Hu et al. [8]. The most interesting feature about C14-type Laves hydrogen storage materials is that they have favourable hydrogen absorption/desorption kinetics, exhibiting easy penetration of hydrogen atoms [20]. For Pd-coated alloy, two sharp diffraction peaks of much higher intensities than those of $\text{TiMn}_{1.52}$ alloy appear at $2\theta = 30.56^\circ$ and $2\theta = 31.83^\circ$. The peaks are attributed to (021) and (040) reflections of phosphorus structure, respectively [21]. The phosphorus was impregnated into the Pd layer during plating of the NaH_2PO_2 -derived Pd layer. In addition, another two peaks appeared at $2\theta = 62.49^\circ$ and $2\theta = 64.82^\circ$. Crystallite sizes of the two alloys were calculated using Scherrer's equation (Equation (2)) [22], where the peak at $2\theta = 40.05^\circ$ was used as a representative peak.

$$\tau = (\kappa\lambda) / \beta \cos(\theta) \quad (2)$$

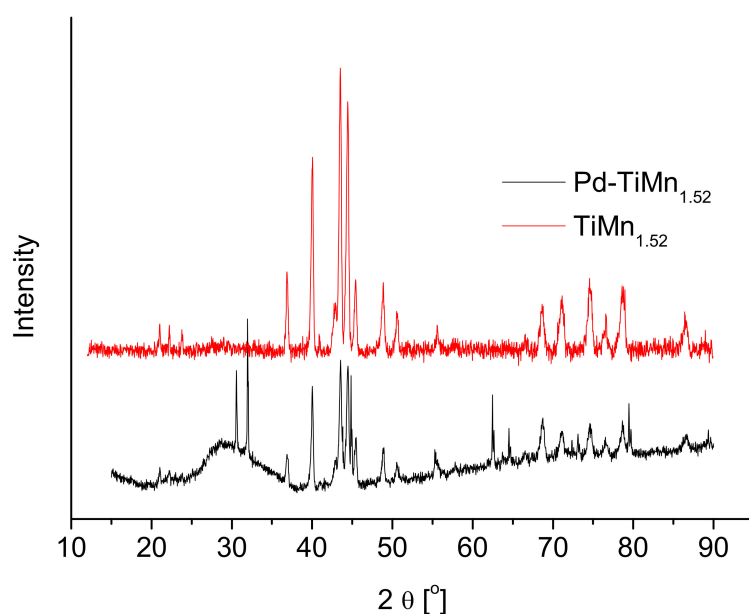


Figure 1. X-ray diffractograms of $\text{TiMn}_{1.52}$ and Pd- $\text{TiMn}_{1.52}$.

Both the uncoated and Pd-coated alloys were found to have the same crystallite size of 29 nm, suggesting that there was no admixing/incorporation between palladium nanoparticles and the bulk TiMn_{1.52} alloy.

3.2. Morphological and Elemental Characterisations

Figure 2 presents SEM images of TiMn_{1.52} before and after surface coating by autocatalytic palladium deposition. The uncoated alloy exhibited a relatively smooth surface, which was occupied by irregular-shaped particles varying in size from 1 to 8 µm. A particle size distribution histogram of the material indicated that the majority of the particles had a size of 1 µm. The alloy may be classified as a nonporous material. For the sample coated with Pd, a discontinuous layer of near-spherical Pd particles was observed. Moreover, the layer seemed to be very dense and uniform. A particle size distribution histogram (Figure 2f) estimated that this alloy had particles ranging in size from 50 to 475 nm, while the majority of the particles had a particle size of 200 nm.

EDS analyses (Figure 3) were employed in parallel to the SEM studies in order to determine the elemental compositions of the alloys. Table 1 shows that EDS data correspond very well with the targeted composition of TiMn_{1.52} alloy, indicating a successful admixing of Ti and Mn metals (ratio of 1:1.52) through the arc melting process.

Table 1. Elemental composition data of TiMn_{1.52} alloy.

Material	Element	EDS Data		Target Composition
		Net Counts	Wt.%	Wt.%
TiMn _{1.52}	Ti	10.25	37.00	36.44
	Mn	9.7	63.00	63.56
	Total	-	100	100

The EDS of Pd-coated alloy (Figure 3b) reveals that the impurities are phosphorus, carbon, and tin at a level of 0.70, 2.31, and 4.54 wt.%, respectively. The presence of these impurities may have resulted from palladium–tin (Pd–Sn) colloidal solution during sensitisation and activation of AB₂ alloys as well as from the NaH₂PO₂-based plating bath during autocatalytic deposition of palladium. When comparing the EDS graphs (Figure 3a,b) of the two alloys, we observe that the net counts of Ti and Mn decreased from 10.25 and 9.7 to 0.9 and 1.5, respectively. This observation may be attributed to a successful palladium loading that covered most part of the alloy surface with a net count of 4.8, as witnessed in the EDS data.

3.3. Hydrogen Absorption Kinetics

Studies of the hydrogenation performances of both uncoated and Pd-coated TiMn_{1.52} alloy were conducted after pre-exposure to air and after preactivation by vacuum heating. The hydrogenation kinetic curves are presented in Figure 4. In addition, Table 2 presents the results obtained through fitting of the experimental data on the Avrami–Erofeev model, which is described here [17]. Without vacuum activation, the uncoated TiMn_{1.52} alloy exhibits slow hydrogen absorption, accompanied by a long incubation period of ~5 min. This is attributed to the presence of a poisonous oxide film on the surface, which causes difficulties in transportation of atomic hydrogen into the bulk alloy. An index of power of 1.37 (Table 2) signifies that hydrogen absorption for unmodified TiMn_{1.52} alloy without activation is controlled by nucleation and growth mechanisms.

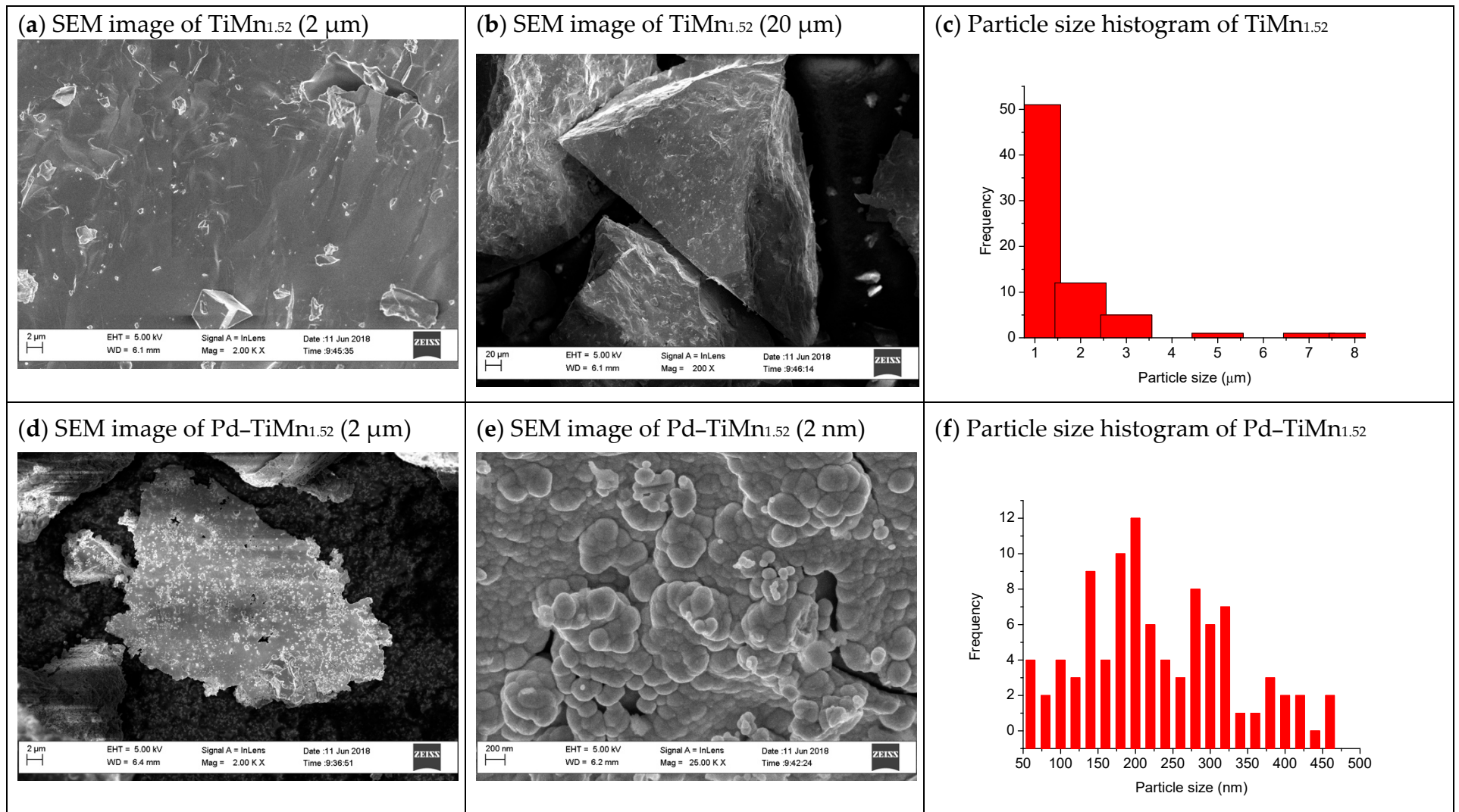


Figure 2. Scanning electron microscope (SEM) micrographs of (a,b) $\text{TiMn}_{1.52}$ and (d,e) Pd- $\text{TiMn}_{1.52}$ and their particle size distribution histograms ((c) $\text{TiMn}_{1.52}$ and (f) Pd- $\text{TiMn}_{1.52}$).

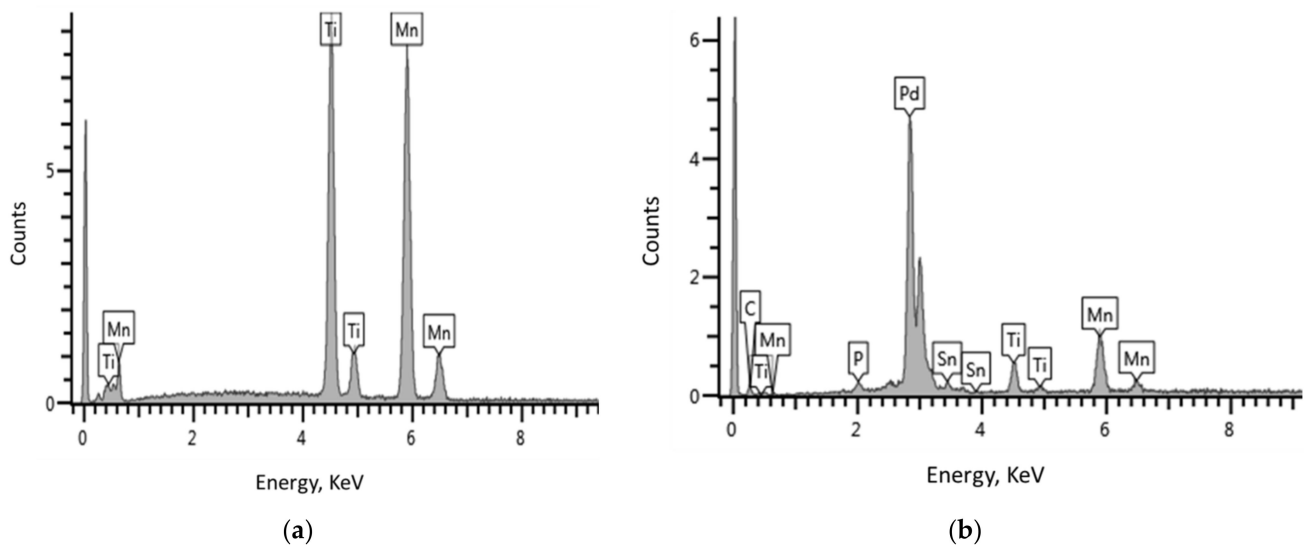


Figure 3. Energy dispersive spectroscopy (EDS) plots of (a) TiMn_{1.52} and (b) Pd-TiMn_{1.52}.

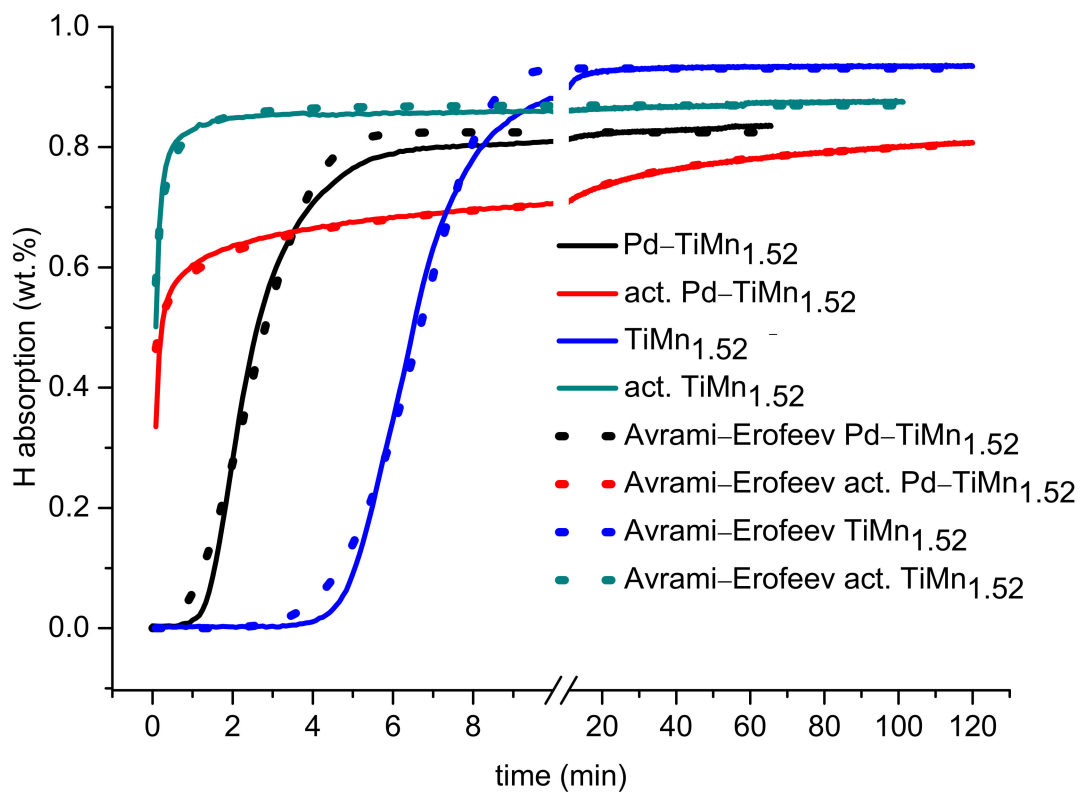


Figure 4. Dynamics of hydrogen absorption ($T = 20\text{ }^{\circ}\text{C}$, $P_{\text{H}_2} = 30\text{ bar}$) by uncoated and Pd-coated AB₂ alloys after pre-exposure to air and after preliminary activation (vacuum heating).

Upon activation in a vacuum by heating at $300\text{ }^{\circ}\text{C}$ for 2 h, the hydrogenation kinetics of TiMn_{1.52} alloy significantly improved and this was supported by the sudden increase of rate constant from 0.438 to 13.2 min^{-1} (Table 2). This is due to the fact that vacuum heating results in the removal of any oxide layers, producing a fast hydrogen-absorbing surface. However, the maximum hydrogen absorption capacity for the activated uncoated alloy was found to be lower than that for the nonactivated uncoated alloy, as depicted in Table 2. Subsequently, the maximum hydrogen absorption capacity continued to drop after

electroless Pd coating. A similar trend was observed by Davids et al. [23] when loading Pd on a TiFe alloy surface.

Table 2. Fit of the experimental data for hydrogen absorption by nonactivated and activated materials using the Avrami–Erofeev equation.

Material	$\left(\frac{H}{AB^2}\right)_{\max}$ (wt.%)		Rate Constant, k (min^{-1})		Index of Power, n	
	Non-activated	Activated	Non-activated	Activated	Non-activated	Activated
TiMn _{1.52}	0.933	0.869	0.438	1.05	1.37	0.50
Pd–TiMn _{1.52}	0.827	0.779	0.771	13.2	0.925	0.50

Loss in hydrogen absorption capacity after Pd coating may be attributed to a large metal (Pd) loading on the surface of TiMn_{1.52} alloy. Li et al. [24] recommended that in order to avoid losses in hydrogenation behaviour, the total weight of PGMs during surface modification of metal hydride-forming alloy through PGMs should be in trace amounts (≤ 0.1 wt.%). In our case, EDS analysis revealed more than 0.1 wt.% of Pd particles on the surface of TiMn_{1.52} alloy, and a decrease in maximum hydrogen absorption capacity was observed upon Pd deposition. In addition, the presence of impurities such as Sn and C on the surface of Pd-coated alloy might have hindered complete hydrogen absorption by the material. Although a decrease in hydrogen capacity was observed, there was an improvement in hydrogenation kinetics, carried out without activation by vacuum heating, upon Pd-coating. The enhancement can be attributed to the partial removal of surface oxide films upon autocatalytic deposition of palladium as well as to the catalytic activity of Pd(P) nanoparticles facilitating splitting of hydrogen molecules into hydrogen atoms. The incubation period is shorter for the alloy coated with Pd.

After vacuum heating, the surface coated alloy exhibited faster hydrogen absorption performances without the presence of an incubation period as compared to the surface coated alloy without vacuum heating. Its hydrogenation kinetics are slower than for activated unmodified TiMn_{1.52} alloy. This is supported by a higher rate constant of activated unmodified alloy ($k = 13.2 \text{ min}^{-1}$) as compared to that of activated modified alloy ($k = 1.05 \text{ min}^{-1}$). The activated uncoated alloy together with inactivated and activated Pd-coated alloys all exhibited an index of power of between 0.5 and 1. Therefore, their interaction with hydrogen is controlled by the nucleation mechanism.

4. Conclusions

This study presents the effect of autocatalytic deposition of palladium on the structure, morphology, and hydrogenation kinetics of TiMn_{1.52} alloy. The study demonstrates that surface modification of TiMn_{1.52} alloy through Pd deposition results in the formation of a discontinuous layer of Pd nanoparticles on the surface of the alloy, thus causing relatively improved activation performances and hydrogen absorption kinetics even after exposure to air. The effect was attributed to improved H₂ dissociation on Pd nanoparticles. The maximum hydrogen absorption capacity of the material decreased upon Pd deposition, and this was associated with a large metal loading on the surface.

Author Contributions: Conceptualization, M.V.L. and K.D.M.; methodology, M.W.D.; software, M.W.D.; validation, M.V.L., K.D.M. and M.J.H.; formal analysis, T.R.S.; investigation, T.R.S.; resources, M.V.L.; data curation, T.R.S.; writing—original draft preparation, T.R.S.; writing—review and editing, K.D.M. and M.J.H.; visualization, M.W.D.; supervision, M.V.L., K.D.M. and M.J.H.; project administration, K.D.M.; funding acquisition, K.D.M. and M.J.H. All authors have read and agreed to the published version of the manuscript.

Funding: This research was funded by the National Research Foundation of South Africa, NRF UID: 118113 (K.D.M.), 116278 (M.W.D.), 132454 (M.V.L.) and 117727 (M.J.H.).

Institutional Review Board Statement: Not applicable.

Informed Consent Statement: Not applicable.

Data Availability Statement: Data is contained within the article.

Conflicts of Interest: The authors declare no conflict of interest.

References

1. Liu, P.; Xie, X.; Xu, L.; Li, X.; Liu, T. Hydrogen storage properties of (Ti 0.85 Zr 0.15) 1.05 Mn 1.2 Cr 0.6 V 0.1 M 0.1 (M=Ni, Fe, Cu) alloys easily activated at room temperature. *Prog. Nat. Sci. Mater. Int.* **2017**, *27*, 652–657. [\[CrossRef\]](#)
2. Somo, T.R.; Maponya, T.C.; Davids, M.W.; Hato, M.J.; Lototsky, M.V.; Modibane, K.D. A comprehensive review on hydrogen absorption behaviour of metal alloys prepared through mechanical alloying. *Metals* **2020**, *10*, 562. [\[CrossRef\]](#)
3. El-eskandarany, M.S.; Al-Ajmi, F.; Banyan, M.; Al-duweesh, A. Synergic effect of reactive ball milling and cold pressing on enhancing the hydrogen storage behavior of nanocomposite. *Int. J. Hydrog. Energy* **2019**, *44*, 26428–26443. [\[CrossRef\]](#)
4. Park, C. Volume expansion of TiMn₂-type hydrogen storage alloy with hydrogenation. *Trans. Korean Hydrog. New Energy Soc.* **2017**, *28*, 459–464.
5. Xu, S.-D.; Fang, L.; Ding, X.-L. Effect of structural factors on the hydrogen storage capacity of nonstoichiometric TiMn_x alloys. *Acta Physicochim. Sin.* **2016**, *32*, 780–786. [\[CrossRef\]](#)
6. Zhu, J.; Dai, L.; Yu, Y.; Cao, J.; Wang, L. A direct electrochemical route from oxides to TiMn₂ hydrogen storage alloy. *Chin. J. Chem. Eng.* **2015**, *23*, 1865–1870. [\[CrossRef\]](#)
7. Davids, M.; Martin, T.; Lototsky, M.; Denys, R.; Yartys, V. Study of hydrogen storage properties of oxygen modified Ti- based AB₂ type metal hydride alloy. *Int. J. Hydrog. Energy* **2020**, *5*, 215. [\[CrossRef\]](#)
8. Hu, T.; Huang, X.; Li, J.; Zhang, J.; Cai, G.; Jin, Z. Experimental investigation and thermodynamic calculation of Ti-Hf-Mn system. *Calphad Comput. Coupling Phase Diagr. Thermochem.* **2020**, *70*, 101776. [\[CrossRef\]](#)
9. Cui, R.; Yang, C.; Li, M.; Jin, B.; Ding, X.; Jiang, Q. Enhanced high-rate performance of ball-milled MmNi_{3.55}Co_{0.75}Mn_{0.4}Al_{0.3} hydrogen storage alloys with graphene nanoplatelets. *J. Alloys Compd.* **2017**, *693*, 126–131. [\[CrossRef\]](#)
10. Dymek, M.; Nowak, M.; Jurczyk, M.; Bala, H. Encapsulation of La_{1.5}Mg_{0.5}Ni₇ nanocrystalline hydrogen storage alloy with Ni coatings and its electrochemical characterization. *J. Alloys Compd.* **2018**, *749*, 534–542. [\[CrossRef\]](#)
11. Somo, T.R.; Mabokela, T.E.; Teffu, D.M.; Sekgobela, T.K.; Hato, M.J.; Modibane, K.D. Review on the effect of metal oxides as surface coatings on hydrogen storage properties of porous and non-porous materials. *Chem. Pap.* **2021**, *10*, 1–15. [\[CrossRef\]](#)
12. Eftekhari, A.; Fang, B. Electrochemical hydrogen storage: Opportunities for fuel storage, batteries, fuel cells, and supercapacitors. *Int. J. Hydrog. Energy* **2017**, *42*, 25143–25165. [\[CrossRef\]](#)
13. Williams, M.; Lototsky, M.; Davids, M.; Linkov, V.; Yartys, V.; Solberg, J. Chemical surface modification for the improvement of the hydrogenation kinetics and poisoning resistance of TiFe. *J. Alloys Compd.* **2011**, *509*, S770–S774. [\[CrossRef\]](#)
14. Bratanich, T.I.; Bulanov, V.N.; Skorokhod, V.V.; Klimenko, V.P. Reversible hydriding of LaNi_{5-x}Al_x-Pd composite in the presence of carbon monoxide. *Powder Metall. Met. Ceram.* **2001**, *39*, 575–583. [\[CrossRef\]](#)
15. Zaluski, L.; Zaluska, A.; Tessier, P.Y.; Ström-Olsen, J.; Schulz, R. Catalytic effect of Pd on hydrogen absorption in mechanically alloyed Mg₂Ni, LaNi₅ and FeTi. *J. Alloys Compd.* **1995**, *217*, 295–300. [\[CrossRef\]](#)
16. Uchida, H.; Wulz, H.-G.; Fromm, E. Catalytic effect of nickel, iron and palladium on hydriding titanium and storage materials. *J. Less Common Met.* **1991**, *172–174*, 1076–1083. [\[CrossRef\]](#)
17. Williams, M.; Lototsky, M.; Nechaev, A.; Yartys, V.; Solberg, J.K.; Denys, R.V.; Linkov, V.M. Palladium mixed-metal surface-modified AB₅-type intermetallics enhance hydrogen sorption kinetics. *South Afr. J. Sci.* **2010**, *106*, 6. [\[CrossRef\]](#)
18. Modibane, K.; Lototsky, M.; Davids, M.; Williams, M.; Hato, M.; Molapo, K. Influence of co-milling with palladium black on hydrogen sorption performance and poisoning tolerance of surface modified AB₅-type hydrogen storage alloy. *J. Alloys Compd.* **2018**, *750*, 523–529. [\[CrossRef\]](#)
19. Dekhtyarenko, V.; Pryadko, T.; Savvakina, D.; Bondarchuk, V.; Mogylnyy, G. Hydrogenation process in multiphase alloys of Ti-Zr-Mn-V system on the example of Ti_{42.75}Zr₂₇Mn_{20.25}V₁₀ alloy. *Int. J. Hydrog. Energy* **2021**, *46*, 8040–8047. [\[CrossRef\]](#)
20. Ha, T.; Lee, S.-I.; Hong, J.; Lee, Y.-S.; Kim, D.-I.; Suh, J.-Y.; Cho, Y.W.; Hwang, B.; Lee, J.; Shim, J.-H. Hydrogen storage behavior and microstructural feature of a TiFe-ZrCr₂ alloy. *J. Alloys Compd.* **2021**, *853*, 157099. [\[CrossRef\]](#)
21. Sarswat, P.K.; Sarkar, S.; Cho, J.; Bhattacharyya, D.; Free, M.L. Structural and electrical irregularities caused by selected dopants in black-phosphorus. *ECS J. Solid State Sci. Technol.* **2016**, *5*, Q3026–Q3032. [\[CrossRef\]](#)
22. Sheikh, A.M.; Silva, E.L.; Abellah, M.Y. Pd-based catalysts for ethanol oxidation in alkaline electrolyte. *Am. J. Min. Metall.* **2014**, *2*, 64–69. [\[CrossRef\]](#)
23. Davids, M.W.; Lototsky, M.; Nechaev, A.; Naidoo, Q.; Williams, M.; Klochko, Y. Surface modification of TiFe hydrogen storage alloy by metal-organic chemical vapour deposition of palladium. *Int. J. Hydrog. Energy* **2011**, *36*, 9743–9750. [\[CrossRef\]](#)
24. Li, B.; Kado, S.; Mukainakano, Y.; Miyazawa, T.; Miyao, T.; Naito, S.; Okumura, K.; Kunimori, K.; Tomishige, K. Surface modification of Ni catalysts with trace Pt for oxidative steam reforming of methane. *J. Catal.* **2007**, *245*, 144–155. [\[CrossRef\]](#)